Journal of Power Sources 208 (2012) 288–295

Contents lists available at SciVerse ScienceDirect

Journal of Power Sources

journal homepage: www.elsevier.com/locate/jpowsour

Preparation, characterization and degradation mechanisms of PtCu alloy nanoparticles for automotive fuel cells

A. Marcu[a,*], G. Toth[a], R. Srivastava[a,b], P. Strasser[b]

[a] Daimler AG, Automotive Fuel Cells Research and Development Centrum, Kirchheim-Nabern, Germany
[b] The Electrochemical Energy, Catalysis, and Materials Science Laboratory, Technical University Berlin, Germany

ARTICLE INFO

Article history:
Received 14 December 2011
Received in revised form 14 February 2012
Accepted 17 February 2012
Available online 25 February 2012

Keywords:
PtCu synthesis
Cathode catalysts
Fuel cells
Evaluation standard
Degradation mechanism
Electrochemical characterization

ABSTRACT

Electrochemically dealloyed PtCu alloy nanoparticles successfully meet the automotive technology target of having four times higher Pt mass activity for the electroreduction of molecular oxygen compared to current state-of-the-art platinum catalysts [1]. However, the catalysts must also maintain their activity throughout the aggressive automotive drive-cycles in order to be implemented in fuel cells cars. Here, the durability of dealloyed PtCu catalysts was systematically evaluated under various voltage-cycles using a rotating ring disk electrode. The stability of the non-noble metal alloy component was proven at electrode potentials below 0.6 V. The platinum stability was evaluated at potentials up to 1.1 V to avoid carbon corrosion and then up to 1.2 V to be closer to the more aggressive cycles developed in startup/shutdown events of the fuel cells. The major known failure modes such as non-noble metal dissolution, platinum dissolution, and particle growth/agglomeration were monitored in order to understand closely the PtCu nanoparticles behavior under different potential cycles and to provide a degradation fingerprint.

1. Introduction

Cost-competitive fuel cells vehicles require cheap and durable cathode catalyst for oxygen reduction reaction (ORR). In the last decade, Pt particles modified with a second metal resulting in Pt-alloy or Pt core–shell catalysts, allow fuel cell operation having low noble metal loading thus lower costs of the system [1,2]. However, if the platinum-based particles cannot maintain their structure over the lifetime of the fuel cell, changes in the morphology of the bimetallic catalyst are likely to result in a loss of electrochemical activity. One of the main issues of the Pt-alloy systems is the non-noble metal stability [3]. Leaching of the non-noble metal in Pt-alloys occurs, since base-metals are thermodynamically unstable under polymer electrolyte membrane fuel cell (PEM FC) potentials in acidic electrolytes [4]. Therefore, a pre-leaching of the alloys in acidic media was proposed by Mukerjee and Srinivasan to minimize the contamination of the membrane with base-metals precipitate [5]. Ball et al. [6] showed that the pre-leaching process removes the non-noble metals only from the 1 to 2 surface layers of the particles, resulting in Pt-skeleton catalysts [7–9]. However, under normal fuel cells operations (0.4 V and 0.9 V) pre-leached Pt-alloy catalysts would experience further base-metals loss as an effect of the potentials conditions [10].

A new preparation method by voltammetric dealloying was developed [11–13] to provide more stable electrocatalysts systems. The dealloying process originates from the phenomenon of corrosion [14–18] but recently it has been proved to be a highly controllable route to nano-structured core–shell catalysts [19–24]. A deliberate partial electrochemical dissolution of the less noble components Cu atoms is achieved, resulting in Pt-enriched shell and alloy core nanoparticle catalysts. Dealloyed PtCu nanoparticles were studied intensively and showed ORR mass activity enhancements of 5 times compared to carbon supported Pt nanoparticles [11,12]. This great achievement alone is not sufficient to employ the catalysts in fuel cell stacks, another important aspect that must be address is catalysts durability. Although fuel cells catalysts performance loss is unavoidable, the degradation rate could be minimized based on a better understanding of the relevant failure mode affecting the stability. In addition to the idle load-cycles occurring during the vehicle life time, the cathode catalysts are exposed as well to more stressful conditions like startup/shutdown [25,26]. Under these conditions, besides the leaching of the non-noble metals, the catalysts may lose activity due to a decay of the electrochemical surface area. In general the Pt electrochemical surface area (ECSA) loss could be caused by Pt dissolution and Pt particle growth or agglomeration, which could be the effect of migration/coalescence or carbon corrosion [27]. Therefore, in order to develop cathode catalysts with tailor-made properties for automotive fuel cells it is extremely important to elucidate the existing knowledge gaps regarding the Pt-alloys degradation mechanisms. The purpose of

* Corresponding author. Tel.: +49 1748 710813; fax: +49 7113 052121269.
E-mail address: alina.marcu@web.de (A. Marcu).

0378-7753/$ – see front matter © 2012 Elsevier B.V. All rights reserved.
doi:10.1016/j.jpowsour.2012.02.065

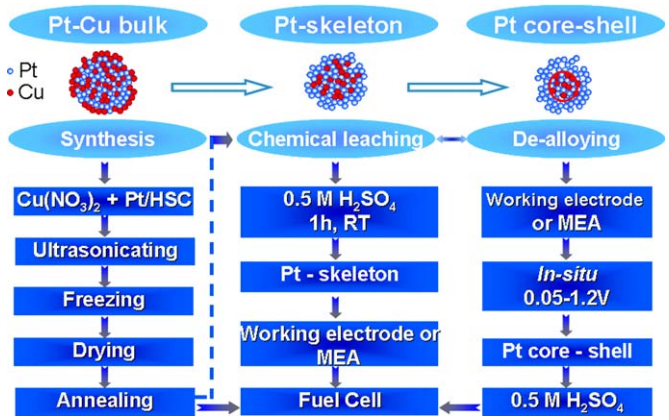

Fig. 1. Profiles of consecutive steps for the preparation of three different systems PtCu bulk alloy, skeleton and core–shell. After synthesis of PtCu alloy in the first column, the bulk alloy can be directly used as cathode catalysts in the fuel cell system, or it could be chemically leached to a Pt skeleton structure as in the second column, or electrochemically dealloyed in the third column to a core–shell. Pt-skeleton could also be used directly as cathode but under fuel cell conditions will become a core–shell.

this research is to clarify the stability of copper platinum catalysts and establish the basic data for formulation of catalysts composition for fuel cells applications. The degradation fingerprint method developed recently in Daimler [28] for evaluation of catalysts under severe simulated fuel cell operation conditions had to be employed. The knowledge achieved in this research constitutes the basis for the pre-selection of cathode catalysts with potential interest for employing in fuel cells for electromobility.

2. Experimental

2.1. Catalyst preparation

In this research three different systems PtCu alloy bulk, Pt-skeleton and PtCu core–shell were prepared following the consecutive steps given in Fig. 1. Carbon supported 22 wt.% PtCu bulk alloy was prepared according with literature [11,29–32] by an impregnation/freeze drying route and annealing following the first column steps in Fig. 1. Preparation started with impregnation and sonication of a commercial 28.1 wt.% Pt/HSC catalyst (Tanaka Kikinzoku International, Inc.) with aqueous metal–salt solutions ($Cu(NO_3)_2$, Sigma–Aldrich, Inc.). The stoichiometry between Pt and Cu was optimized to 1:3 ratio. Once the slurry was sonicated, the impregnated catalysts were frozen in liquid N_2 and subsequently freeze-dried under a moderate vacuum. Reduction and alloying of Pt with Cu on the carbon support was thermally driven under a reductive H_2 atmosphere (4% H_2, Ar balance) using a Lindberg/Blue tube furnace at temperatures of 800 °C for 7 h. Commercially available Pt/HSC was also exposed to an H_2 atmosphere at 800 °C to aid in comparisons of ECSA loss. This procedure has been shown to be an effective strategy to modify the surface electrocatalytic reactivity of Pt bimetallic nanoparticles [13,31–37]. The alloy prepared is further chemically leached to a Pt-skeleton structure or electrochemically dealloyed to a core–shell structure. The chemical leaching of the alloys was performed in acidic media. We extended a method for the controlled removal of the non-noble metal Cu from the surface layers of Pt-based alloy nanoparticles following the second column steps in Fig. 1. The 22 wt.% PtCu catalyst was leached in 0.5 M H_2SO_4, at room temperature for 1 h. To assure that 1 h was enough to remove the Cu ions that were not alloyed and/or from the surface of the catalyst particles, a further leaching was performed for 24 h. Afterwards, the leaching media was analyzed for the dissoluted Cu amount. The electrochemical dealloying process was performed using a rotating ring disk electrode (RRDE), according to literature [11] and following the third column in Fig. 1. The working electrode was swept repeatedly at 1000 mV s^{-1} for 200 cycles between 0.05 and 1.1 V, until the hydrogen adsorption area became stable and similar to a Pt/C surface. A second potential window between 0.05 and 1.2 V was proposed and used for the dealloying in this research. In order to understand the effect of the voltage window proposed over the dealloying process, a comparative study was initially performed. The potential window of 0.05–1.2 V was compared with 0.05–1.0 V previously reported in literature [11]. During the dealloying the Cu atoms leaches out from the PtCu precursor material, diffusing in the liquid electrolyte 0.5 M H_2SO_4 that was removed and exchanged with fresh electrolyte before each degradation test.

2.2. Thin film electrode preparation

A catalyst ink was prepared by ultrasonicating 15 min an aqueous solution corresponding to 2 mg catalyst cm^{-3} deionized water [38–41]. The Pt loading on the working electrode of 28 $\mu g_{Pt}\ cm^{-2}_{electrode}$ was achieved by dispersing the corresponding amounts of suspension onto a 5 mm diameter mirror-polished glassy carbon disk (Sigradur GmbH, Germany). After the catalyst thin-film has dried under nitrogen, an aqueous Nafion solution was added over the catalysts film, according to the method proposed by Schmidt et al. [42]. Since the Nafion film has a low thickness, its diffusion resistance is negligible [42]. After the Nafion film was dried in nitrogen, the working electrode was transferred to a RRDE. In this study the initial state of the platinum is considered after the electrocatalyst was either voltammetrically dealloyed or chemically leached.

2.3. Stability tests

To better understand the behavior of PtCu catalysts under fuel cell operating conditions, three different testing protocols were considered using RRDE. Firstly, the stability of the less noble metal Cu was investigated under low potential windows 0.05–0.6 V for both Pt-skeleton and Pt core–shell catalyst. Secondly, the catalysts stability was investigated under 0.6–1.1 V and 0.6–1.2 V. The cycling measurements were triangle wave cycling at a scan rate of 1 V s^{-1}, for 10,000 cycling. Stopping at 0, 500, 1000, 2000, 5000, 8000, 10,000 cycles in order to measure the surface area and the ORR, as well to collect the working electrolyte to be analyzed for Pt and Cu content.

2.4. RRDE measurements

The electrochemical measurements were performed in a three-compartment electrochemical cell setup. A Pt wire and a hydrogen reference electrode were used as counter and reference electrode, respectively. The working electrode was installed into a commercial ring disk head with an exchangeable disk of 5 mm, surrounded by an insulating Teflon U-cup and embedded Pt ring. The potentials were controlled by a bi-potentiostat (Pine Instruments). The electrolyte used was 0.5 M H_2SO_4. All measurements were conducted at room temperature. At the beginning of electrochemical measurements, the electrocatalysts were immersed into the electrolyte under potential control and held at 0.05 V, in a deaerated N_2 atmosphere electrolyte. The ECSA of each catalyst sample was determined using the mean integral charge area of the hydrogen underpotentially deposited (H_{upd}). The measurements scan rate was 10 mV s^{-1} at room temperature and the charge used to determine the ECSA was of 210 $\mu C\ pro\ cm^2_{Pt}$, assuming the hydrogen coverage of 0.77 ML [43,44]. The normalized kinetic ORR currents

at the disk electrode given as active mass or specific kinetic ORR currents were determined from Tafel plots.

2.5. Elemental and structural analysis

The amount of dissolved cupper and platinum from the working electrode in to the electrolyte was determined by Inductively Coupled Plasma Mass Spectroscopy (ICP-MS) with a platinum detection limit of 0.001 mg l^{-1}. The electrolyte sampling was collected at 0, 500, 1000, 2000, 5000, 8000, 10,000 cycles for analysis.

Transmission electron microscopy (TEM) images were obtained using a Philips CM 20 microscope operated at 200 kV. Particle size and size distribution was obtained in the beginning and end of the measurements counting 500 particle per sample.

3. Results and discussion

3.1. Catalyst formulation

A new method, the voltammetric dealloying, was proposed for the preparation of catalysts with high potential for fuel cells applications [45] and it was closely investigated in our group because of its advantages. The method successfully solves two very important issues for the automotive fuel cells industry. The first advantage is the increased catalytic activity is increased by a factor of 5 compared to Pt/C state-of-the-art catalysts, achieving the required fuel cells vehicles targets for cathode catalysts. The second advantage is the increased stability of the transitional metal, due to formation of a Pt-shell that protects the Cu from leaching out. Nevertheless, the preparation of the membrane electrode assembly (MEA) catalyst layers for application in PEMFC requires additional steps. PtCu bulk alloy are first applied to a polymeric membrane as a cathode layer and assembled in a cell. The MEA is then subjected to voltammetric cycling while the Cu ions are selectively removed from the precursor particles and trapped at the negatively charged SO_3^- inside the membrane. Finally, the membrane electrode is disassembled and immersed in liquid acid to ion exchange the Cu ions with an excess of protons. Due to the post treatment of the MEAs the method follows a systematic which is laborious for large industrial application. A preferred strategy to deliberately modify the surface catalytic properties of Pt-based alloys, for automotive applications is a chemical treatment of the nanoparticles. This method was extended in our group, in which the bimetallic alloy precursor materials were subject to acidic corrosion media. In this way we achieved to remove the Cu atoms from the PtCu nanoparticle surface and to develop a Pt-skeleton. The compared characteristic of the catalyst prepared with both methods is presented in the following.

3.2. Electrochemical stability

The Pt-skeleton sample initially showed low surface area of $43 \pm 5\ m^2\ g_{Pt}^{-1}$ because the Pt surface is blocked by the presence of Cu atoms that were not completely removed during the acid treatment. Nevertheless, as soon as voltage cycling is applied to the sample the Cu atoms starts to leach out and more platinum becomes available for hydrogen interaction resulting in a gradual increase in surface area. Depending on the potential window used, it takes different number of cycles to reach a maximum of $76 \pm 4\ m^2\ g_{Pt}^{-1}$. The leaching rate increases with the upper potential limit and a maximum surface area is reached after 500 cycles when a potential cycling of 0.6–1.1 V was used and after 300 cycles for potentials of 0.6–1.2 V.

In case of the dealloying process two different voltages cycles were applied and compared in Fig. 2, the first 0.05–1.1 V was proposed previously in literature [11] and a second one of 0.05–1.2 V

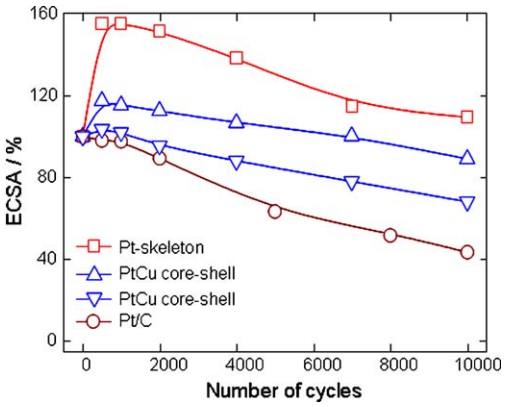

Fig. 2. ECSA loss during potential cycling 0.6–1.1 V with 1 V s^{-1}, in H_2SO_4 for 10,000 cycles of the Pt-skeleton (squares), of the core–shell which was electrochemically dealloyed at 0.5–1.1 V (triangle up) and at 0.5–1.2 V (triangle down) and for Pt/C catalysts (circles).

which was proposed for this research. When 200 dealloying cycles between 0.05 and 1.1 V were applied, the initial surface area found was of $61 \pm 2\ m^2\ g_{Pt}^{-1}$. Considering same 200 numbers of cycles but increasing the upper potential limit to 1.2 V the initials surface area was of $70 \pm 7\ m^2\ g_{Pt}^{-1}$. After the two different dealloying cycles both core–shell systems were exposed to degradation cycles of 0.6–1.1 V. The ECSA for the first core–shell systems increased to a maximum of $74 \pm 7\ m^2\ g_{Pt}^{-1}$ during the first 200 degradations cycles. The second core–shell system reached a maximum surface area of $76 \pm 4\ m^2\ g_{Pt}^{-1}$, after 100 degradation cycles. This behavior suggests that a further Cu leaching with simultaneous roughness of the Pt structure occurs after the dealloying and that the leaching rate increases with the upper potential limit. The leaching rate increases with the upper potential limit. This behavior has also been observed previously in literature [46]. In this research the dealloying potential window used is 0.05–1.2 V considering 200 cycles, since this procedure provides more stable core–shell. The beginning of life is considered to be the maximum surface area reached for each of the catalysts.

The carbon supported platinum which was heat treated to have particle size of 3.6 ± 0.2 nm similar to PtCu catalyst, initially has a surface area of $78 \pm 4\ m^2\ g_{Pt}^{-1}$ similar to the maximum surface $76 \pm 4\ m^2\ g_{Pt}^{-1}$ determined for the core–shell nanoparticles.

In the following we investigated the Cu stability during cycles under potential window of 0.05–0.6 V. Fig. 3 displays the ECSA

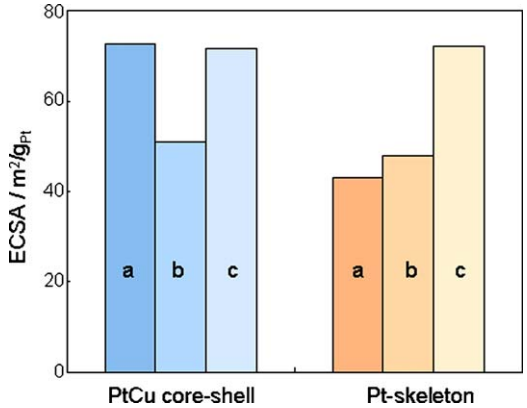

Fig. 3. ECSA losses determined under low potential scans 0.05–0.6 V for core–shell catalyst dealloyed under 0.5–1.2 V and Pt-skeleton where (a) first cycle, (b) after 10,000 cycles, (c) after 400 potential cycling cleaning of 0.5–1.1 V.

loss determined under low potential scans for the core–shell and the Pt-skeleton samples. The low potential window has the purpose to investigate the stability of the second metal Cu without affecting Pt stability. The base-metals are unstable in acidic electrolytes and fuel cells potentials, leaching out of the catalyst particles [3,4]. During potential cycling, the surface area of the core–shell apparently decreases due to Pt surface contamination that usually occurs at these low potentials. Cycling the electrode at higher potentials as 1.1 V, the Pt surface is cleaned and the maximum value of the surface area is recovered. However, the ECSA of the Pt-skeleton sample increases and becomes similar with the core–shell, suggesting further Cu leaching. ICP-MS was used to determine the Pt and Cu composition for the initial bulk alloy, Pt-skeleton and core–shell materials. An initial bulk composition was determined to be of $Pt_{40}Cu_{60}$. During chemical leaching a 33% of initial cupper was lost in the electrolyte while during electrochemical dealloying 67% was removed. After dealloying the nanoparticles composition was determined to be $Pt_{80}Cu_{20}$, in agreement with literature data [29]. After low potential cycling, very small amounts of 0.8 μg Cu were found in the electrolyte, for both core–shell and Pt-skeleton samples. Increasing the upper potential limit to 1.1 V during cleaning, the dissolution of the second metal from Pt-skeleton catalysts occurs and a

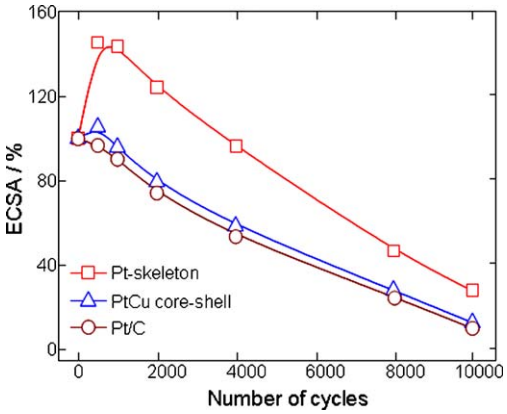

Fig. 4. ECSA losses of the Pt-skeleton (squares), PtCu core–shell dealloyed at 0.5–1.2 V (triangles) and for Pt/C catalysts (circles), during potential cycling 0.6–1.2 V with 1 V s^{-1}, in H_2SO_4 for 10,000 cycles.

2.4 μg_{Cu} was found in the electrolyte. In core–shell catalyst, the noble metal shell protects the non-noble atoms from the core against dissolution and only 0.4 μg Cu were found in electrolyte after cycling.

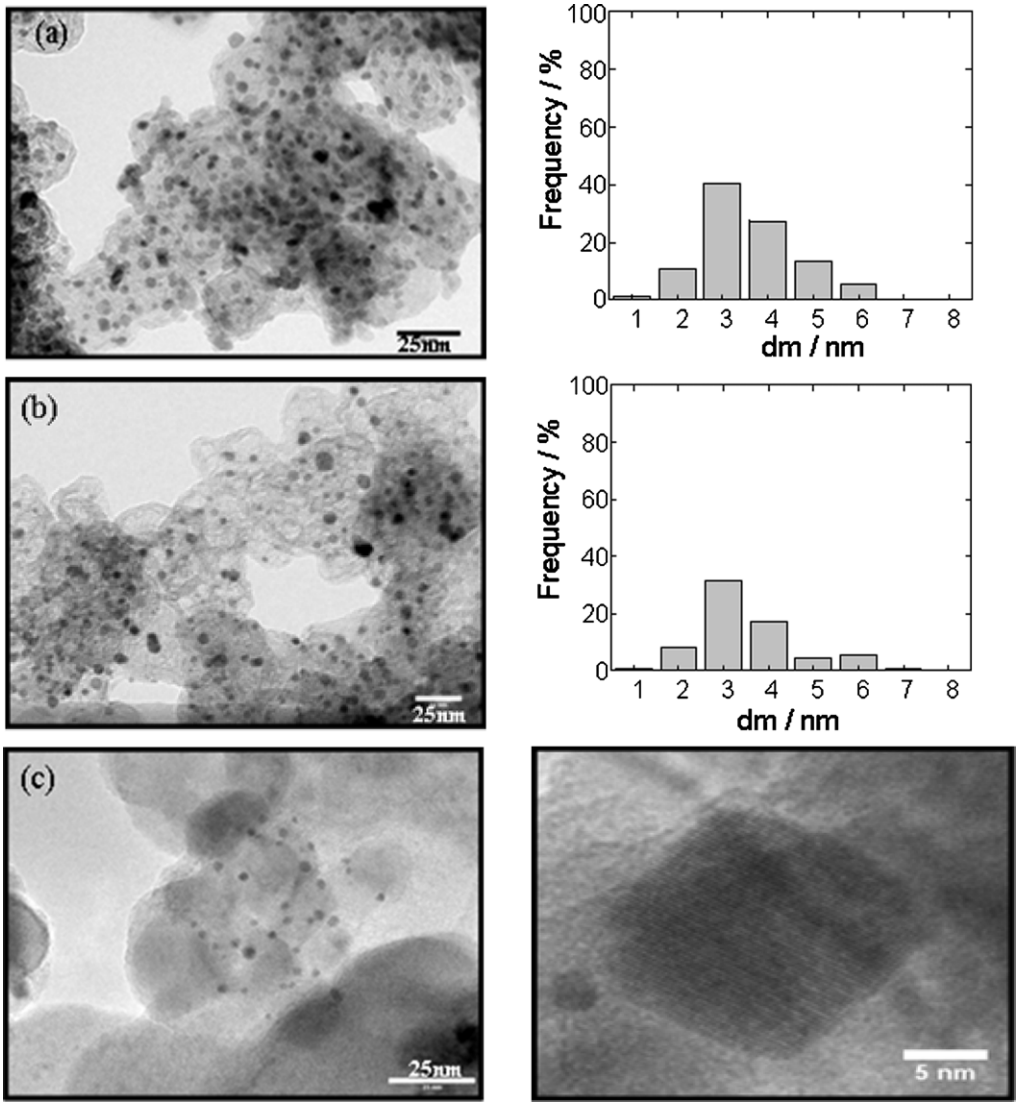

Fig. 5. TEM image and size distribution of (a) PtCu bulk alloy, (b) PtCu core–shell after degradation at 0.6–1.1 V, (c) PtCu core–shell after degradation at 0.5–1.2 V. Both samples were dealloyed at 0.5–1.2 V.

The stability of the PtCu regarding Pt dissolution and agglomeration was investigated under potentials cycling of 0.6–1.1 V and 0.6–1.2 V as illustrated in Figs. 2 and 4. It can be observed that the chemical leaching process affects only the break-in time which is the time it takes the catalyst to obtain its maximum ECSA. After a maximum surface area was reached using 300–500 degradations cycles, the Pt-skeleton behaves similar to Pt core–shell. Nevertheless, the break-in time has a major impact on automotive fuel cells since the second metal that leaches out will be found in the ionomer phase leading to increased kinetic losses, thus lowering fuel cell performance of the MEA [3,47]. It becomes inherently clear from the results that there is a stability advantage of approximately 20% for PtCu catalyst over Pt/C under degradation cycles of 0.6–1.1 V. This advantage comes particularly from alloying the Pt metal with Cu and not as a particle size effect. Both catalysts have similar uniform particle size due to the heat treatment of the Pt/C similar to PtCu catalyst. However, this great advantage is lost by increasing the potential window with 100 mV. Potential cycling up to 1.2 V has from the beginning a higher impact over the catalyst degradation rate. While the total 30% loss of ECSA is obtained at the end of 10,000 cycles under 0.6–1.1 V, it takes only 2000 cycles at 0.6–1.2 V to reach the same value. Furthermore after degradation the Pt-skeleton and core–shell catalysts acts similarly to Pt/C and the overall degradation is ~80% surface area loss. For more detailed insight regarding the trends in ECSA loss, a breakdown of the degradations mechanisms was performed.

3.3. Quantification of the degradation failure modes

Several mechanisms appear to be responsible for the loss of Pt ECSA and the most significant are Pt dissolution and Pt agglomeration/growth [48–51]. To understand which of the mechanism has a bigger impact over the ECSA loss, a quantification of the individual failure mode was performed. TEM was used in order to characterize the particle size at initial and final state as shown in Fig. 5a. Assuming a spherical particle, the mean particle size for all three samples PtCu bulk material, core–shell and Pt-skeleton was found to be similar 3.4 ± 0.6, 3.5 ± 0.1 and 3.8 ± 0.4 nm in good agreement with literature data for PtCu bulk alloy annealed at 800 °C [23]. The mean particle size of the heat treated Pt/C was determined to be 3.6 ± 0.2 nm.

In general TEM analysis gives valuable information regarding the particle size and distribution of Pt on the carbon support; nevertheless they are time and cost consuming. In this research the dispersion was used as a parameter that provides information about the changes in particle size and its relationship to ECSA loss. Based on the known definition, the dispersion is given by the ratio between the active Pt surface atoms and the remained Pt atoms at the working electrode. The latter is determined by subtracting the amount of Pt loss determined from ICP-MS data, from the initial Pt amount at the working electrode. The former is determined applying the flowing relationship:

$$A_{Pt} = \left(\frac{Q_{H_{upd}}}{F} \right) \times N_A$$

where A_{Pt} is the number of active platinum atoms or surface atoms, $Q_{H_{upd}}$ is the hydrogen under potential deposition charge (C) determined from the measured basic voltammograms, F is the faraday constant $F = 96{,}485\ C\ mol^{-1}$ and N_A is the Avogadro constant $6.02 \times 10^{23}\ mol^{-1}$. Therefore, an initial core–shell dispersion experimentally determined $D_E = 0.26$ was found in agreement with the dispersion determined from TEM data $D_{TEM} = 0.29$. Furthermore, the initial core–shell mean particle size, from TEM analysis, of 3.5 ± 0.1 nm corresponds to a theoretical surface area $SA_T = 77 \pm 4\ m^2\ g_{Pt}^{-1}$, in good agreement with the experimental maximum surface area $SA_E = 76 \pm 6\ m^2\ g_{Pt}^{-1}$ determined from H_{upd}.

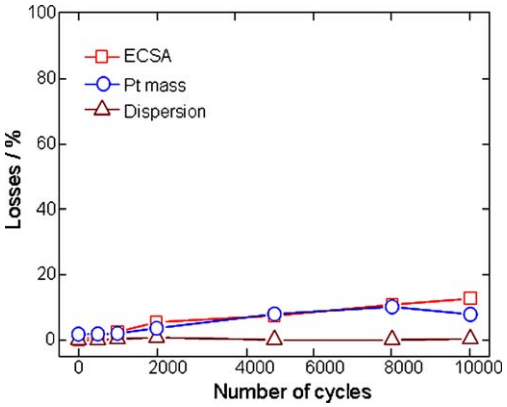

Fig. 6. Breakdown of the different degradation mechanism represented by the losses of ECSA 33% (squares), Pt dissolution 32% (circles) and dispersion 2% (triangles), versus the number of cycles for PtCu core–shell catalysts under potential cycling 0.6–1.1 V. The core–shell was obtained by dealloying at 0.5–1.2 V.

Potential cycling of 0.6–1.1 V for the core–shell catalyst is represented in Fig. 6 showing the losses of ECSA, Pt dissolution and dispersion. The percentage losses are normalized to the corresponding cycling intervals where the process was stopped to collect the electrolyte for ICP analysis. It can be observed that the trend of Pt dissolution is similar to ECSA loss and the change in dispersion is negligible. The total Pt mass loss was approximately 32% and a 30% loss in the ECSA was recorded, while the change in dispersion was only 2%. This behavior leads to the conclusion that the main effect causing the ECSA loss is platinum dissolution. This hypothesis is confirmed by TEM pictures performed at the end of the degradation, Fig. 5b. The mean particle size determined is 3.8 ± 0.4 nm with $D_{TEM} = 0.27$ in good agreement with the dispersion experimentally determined $D_E = 0.26$.

Potential cycling of 0.6–1.2 V for the core–shell catalyst is represented in Fig. 7 showing the losses of ECSA, Pt dissolution and dispersion. The percentage losses are normalized versus the corresponding cycling interval. It is interesting to note that for the first 500 cycles the trace of ECSA loss is similar to dissolution, while the change in dispersion is negligible. Therefore, the decrease in ECSA loss initially is dominated by the dissolution of Pt. After 500 cycles, a small change in the dispersion can be observed, the catalyst particles starts to grow/agglomerate and the contribution of

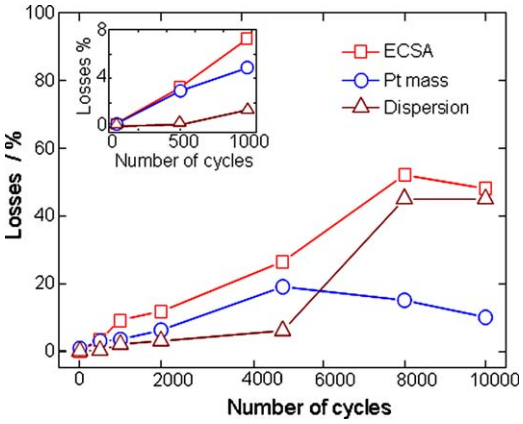

Fig. 7. Breakdown of the different degradation mechanism represented by the losses of ECSA 81% (squares), Pt dissolution 54% (circles) and dispersion 64% (triangles), normalized versus the corresponding number of the cycles of potential cycling 0.6–1.2 V for PtCu core–shell catalysts, which was dealloyed previously at 0.5–1.2 V.

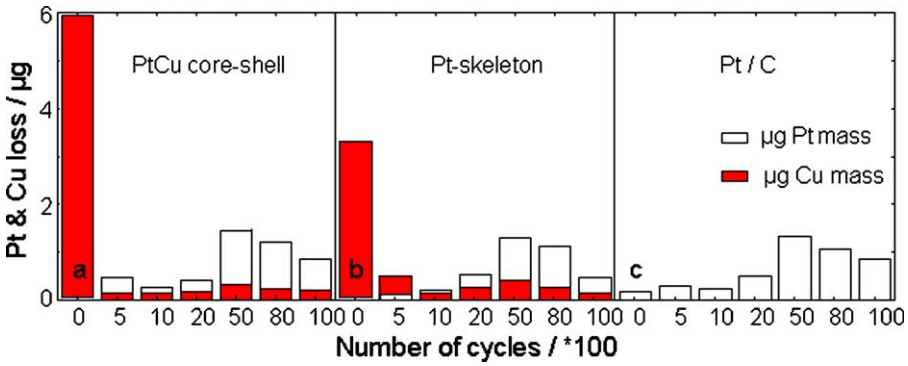

Fig. 8. ICP-MS data of Pt (white columns) and Cu (red columns) atoms lost under potential cycling of 0.6–1.2 V, where (a) represents the Cu lost during dealloying under 0.5–1.2 V, (b) Cu lost during acid chemical leaching, (c) platinum lost during dealloying. (For interpretation of the references to color in this figure legend, the reader is referred to the web version of the article.)

Pt dissolution over the ECSA loss starts to decrease. At the end of the degradation Pt dissolution still occurs but with lower rates as an effect of the particle growth. These results are in agreement with the known behavior that the growth of the platinum particle favors the stability against dissolution [52] and with previous fingerprint data for Pt/C determined under start/stop fuel cell conditions [28]. From the total remaining 46% platinum mass on the electrode, 42% was found to be agglomerated. Therefore, at the end of the degradation cycles the ECSA loss is predominantly affected by growth/agglomeration. During potential cycling, the PtCu catalyst is highly degraded and at the end of 10,000 cycles very few particle are left on the carbon support. These particles are spherical with size of 5 nm and non-spherical agglomerates with a size of 7 nm as illustrated in Fig. 5c. The total Pt mass loss was 81%, with a total 54% of the ECSA loss, while the change in dispersion was 64%. Similar degradation behavior under potential of 0.6–1.2 V was found for Pt/C reference material. Initially the ECSA loss is dominated by Pt dissolution and after 5000 cycles the most dominant failure mode becomes agglomeration/growth of the particle. This behavior as mentioned before is dependent on the initial Pt amount and its distribution on the surface of the support material. At the end of the degradation cycles the losses recorded were 84% for ECSA, 58% for Pt mass and 63% for dispersion. Fig. 8 shows that for Pt/C catalysts the total amount of 4.4 μg_{Pt} Pt loss is comparable to 4.1 μg_{Pt} Pt loss in case of core–shell and to 4.0 μg_{Pt} Pt loss for the Pt-skeleton. Moreover, the trend of Pt dissolution over the number of cycles is similar for all samples Pt/C, Pt-skeleton and core–shell. A great impact over the recorded high loss of the catalysts particle could be, the high surface nature of the carbon supporting material. Linse et al. [47] showed an approximately doubling of the CO_2 concentration evolution from ~6 ppm at 1.1 V to ~13 ppm at 1.2 V for a high surface area carbon Therefore the similarity in Pt mass loss for all three samples could be also the results of carbon corrosion as discussed in literature [45].

The life time behavior of the PtCu nanoparticles under different potentials conditions is illustrated in Fig. 9. Starting from a Pt-bulk alloy (A structure) the nanoparticles could be chemically leached to Pt-skeleton (B structure) or electrochemically dealloyed to Pt core–shell (C structure). The Pt-skeleton under potential cycles is subjected to further Cu leaching leading to Pt core–shells. Based on the behavior of both systems at low 0.05–0.6 V and higher 0.6–1.1 V potentials, discussed previously in this research, it can be concluded that the Cu atoms within the core–shell particle are protected by platinum and do not leach out as long as the Pt shell is not restructured. ICP-MS was performed during the 10,000 degradation cycles at 0.6–1.1 V. A total number of 4×10^{15} Cu atoms, representing 50% loss, were dissoluted in electrolyte, which was slightly smaller compared to 7.5×10^{15} Pt atoms. Considering the initial TEM particle size distribution the provenience of the 30% Pt atoms lost at the end of test, corresponds to 98% dissolution of 1 nm particles and 50% dissolution of 2 nm particles. Assuming spherical particle size, Ostwald Ripening dissolution mechanism [53] and that the 1 nm particle are free of Cu after dealloying, it was estimated that the dissolution of 0.1 ML Pt leads to 16 Cu atoms leaching out from a 2 nm particle. Therefore, once Pt starts dissolute, the Cu will be again prone to leaching.

3.4. Electrocatalytic reactivity

It is already proved that Pt mass and specific activity of the core–shell particles exceeds that of state-of-the-art Pt electrocatalyst by more than a factor of 4 and thus meets performance targets for fuel cell cathode electrodes [2,26,31]. Therefore, in this paper we only focused on how the different potential windows affect the activity of the different PtCu system and more importantly how to quantify the effect of Pt dissolution and agglomeration over the mass activity losses.

The specific and mass activities of the initials state and after degradation of the Pt/C, core–shell and Pt-skeleton are related in Table 1. During low potential cycling of 0.05–0.6 V an apparent increase in the specific activity of the core–shell associated with the decrease in the ECSA due to the adsorption of impurities on the surface was observed. After cleaning at 1.1 V both samples,

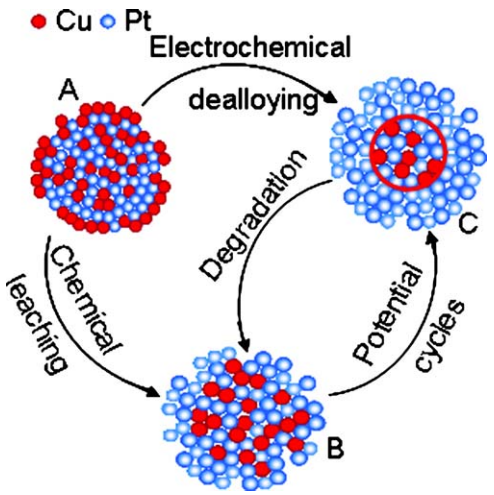

Fig. 9. Behavior of the PtCu as cathode material in fuel cells. PtCu bulk alloy could be leached in acidic media to Pt-skeleton, or electrochemically dealloyed to PtCu core–shell. Pt-skeleton under fuel cell operational condition will develop into a core–shell structure. PtCu core–shell is stable as long as the shell is not restructured.

Table 1
The specific and mass activities of the initials state and after degradation of the Pt/C, PtCu core–shell and skeleton.

	Core–shell	Pt-skeleton	Pt/C
Specific activity ($mA\,cm^{-2}$)			
BoL[a]	0.55	0.60	0.14
EoL[b]@ 0.05–0.6 V	0.55	0.55	0.14
EoL@ 0.6–1.1 V	0.28	0.29	0.14
EoL@ 0.6–1.2 V	0.25	0.24	0.13
Mass activity ($mA\ mg_{Pt}^{-1}$)			
BoL	487	512	138
EoL@ 0.05–0.6 V	470	490	137
EoL@ 0.6–1.1 V	400	403	98
EoL@ 0.6–1.2 V	89	91	61

[a] BoL – beginning of life.
[b] EoL – end of life, after degradation.

the core–shell and Pt-skeleton, showed similar specific and mass activities corresponding to the initial core–shell recorded values, supporting the statement that the Pt shell is protecting the Cu against leaching. Potential cycles of 0.6–1.1 V, showed initially a great advantage for Pt-skeleton with 6× higher specific activity then Pt/C catalyst. However, the activity decreases at the end of the degradation and reaches similar values to the core–shell catalyst. The specific activities of both Pt-skeleton and core–shell, at the end of cycling exhibits 1.5× factor compared to Pt supported bulk catalysts. Similarly, both PtCu samples exhibit the mass activity compared to Pt/C, with a factor of 2.5 at the end of test. Potential cycles as 0.6–1.2 V are in general more stressful for the catalyst stability, leading to accelerated degradation rate as shown above. From the specific and mass activity data it is observed that potentials as 1.2 V have a detrimental effect on the ORR activity. This is likely attributable to the enhanced dissolution/agglomeration probably caused by carbon corrosion.

The quantification of the mass activity losses for Pt/C at 0.9 V normalized to initial catalyst amount, the remained catalyst at the working electrode and to the dispersion factor are displayed in Fig. 10. The total loss considering the initial Pt amount is about 56% being caused by Pt dissolution and agglomeration. Normalizing the ORR current to the remaining Pt amount at the working electrode, the total loss becomes 51% corresponding to agglomeration and growth of the particles. The trace of mass activity normalized versus the remained Pt amount, shows small losses for the first 500 cycles corresponding to the behavior shown previously for PtCu where agglomeration starts after the first 500 cycles. After 5000 cycles the activity loss is enhanced due to agglomeration, becoming the most predominant cause. When normalizing the ORR current to dissolution and dispersion factors, the trace of the mass activity

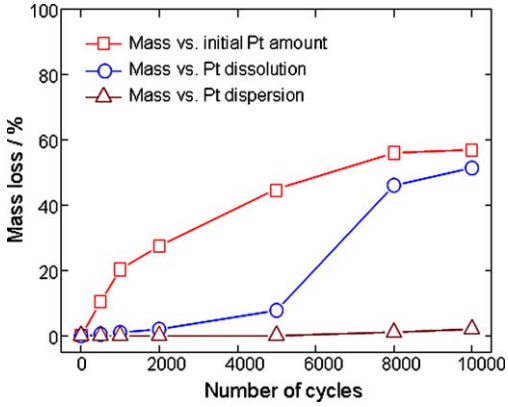

Fig. 10. Mass activity loss of Pt/C catalysts normalized versus initial catalysts amount (empty squares), Pt amount left at the working electrode (circles), and dispersion factor (full squares), considering potential cycling 0.6–1.2 V.

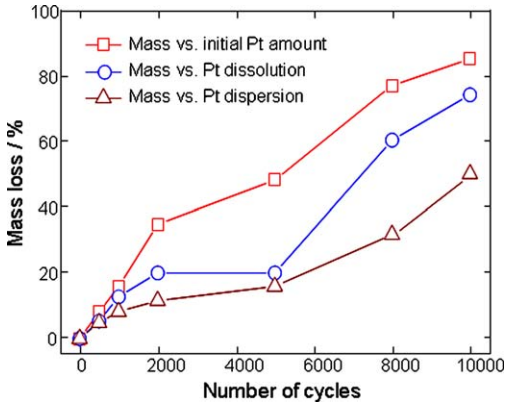

Fig. 11. Mass activity loss of PtCu core–shell, dealloyed at 0.5–1.2 V, normalized versus initial catalysts amount (empty squares), Pt amount at the working electrode (circles), and dispersion factor (full squares), considering potential cycling 0.6–1.2 V.

losses becomes constant and the absolute value of the mass activity corresponds to the initial value 160 $mA\,mg_{Pt}^{-1}$. In case of PtCu core–shell the ORR current after being normalized to Pt dissolution and agglomeration, as illustrated in Fig. 11, is not constant but represents the losses corresponding to the electronic changes within the particles. Therefore, at the end of degradation, 10% of mass activity loss is due to Pt dissolutions, the growth/agglomeration contribute about 25% and 50% are attributed to the deactivation of the core–shell particles.

4. Conclusions

PtCu core–shell nanoparticle electrocatalyst is an important advancement in the development of active cathode catalysts for PEMFCs. In comparison with Pt-skeleton electrocatalysts, they show an additional gain in non-noble metal stability and they are characterized by mass activities of up to a factor of 5 versus carbon supported Pt catalysts.

The degradation fingerprint method developed and utilized here is a practical approach of general applicability for the evaluation and benchmarking of potential catalysts for fuel cell applications. Our data suggests that the non-noble metal inside the core has a good stability against leaching under the applied conditions with the core being very well protected by the Pt shell. We also showed that the Pt dissolution rate is clearly lower in core–shell architectures compared to state-of-the-art carbon-supported Pt nanoparticle. The origin of the enhanced stability could be attributed to the electronic effects and geometric structure of the Pt atoms upon alloying Pt with Cu.

PtCu core–shell catalysts are a promising approach to meet the automotive activity and stability targets under normal driving conditions at open circuit voltage. Nevertheless, the high cathodic potentials developed during startup/shutdown significantly affect the catalysts stability and therefore their implementation in fuel cell stacks. This dependence of the stability on the startup/shutdown conditions imposes the need to develop effective mitigation strategies to avoid high cathode potentials.

References

[1] S. Koh, P. Strasser, J. Am. Chem. Soc. 129 (2007) 12624–12625.
[2] J. Zhang, F.H.B. Lima, M.H. Shao, K. Sasaki, J.X. Wang, J. Hanson, R.R. Adzic, J. Phys. Chem. B 109 (2005) 22701–220704.
[3] A. Gasteiger, S.S. Kocha, B. Sompalli, F.T. Wagner, Appl. Catal. B: Environ. 56 (2005) 9–35.
[4] E. Deltombe, M. Pourbaix, Atlas of Electrochemical Equilibria in Aqueous Solutions, National Association of Corrosion Engineers, Texas, 1974, pp. 322–329.

[5] S. Mukerjee, S. Srinivasan, in: W. Vielstich, A. Lamm, H. Gasteiger (Eds.), Handbook of Fuel Cells – Fundamentals, Technology and Applications, Wiley, Chichester, 2003.
[6] S.C. Ball, S.L. Hudson, J.H. Leung, A.E. Russell, D. Thompsett, B.R.C. Theobald, ECS Trans. 11 (2007) 1247–1257.
[7] V.R. Stamenkovic, B. Fowler, B.S. Mun, G. Wang, P.N. Ross, C.A. Lucas, N.M. Markovic, Science 315 (2007) 493–496.
[8] V.R. Stamenkovic, B.S. Mun, M. Arenz, K.J.J. Mayrhofer, C.A. Lucas, G. Wang, P.N. Ross, N.M. Markovic, Nature 6 (2007) 241–246.
[9] V.R. Stamenkovic, B.S. Mun, K.J.J. Mayrhofer, P.N. Ross, N.M. Markovic, J. Am. Chem. Soc. 128 (2006) 8813–8819.
[10] G.E. Ramirez-Caballero, P.B. Balbuena, Chem. Phys. Lett. 456 (2008) 64–67.
[11] R. Srivastava, P. Mani, N. Hahn, P. Strasser, Angew. Chem. Int. 46 (2007) 8988–8991.
[12] S. Koh, N. Halm, P. Strasser, ECS Trans. 3 (2006) 139–149.
[13] M. Oezaslan, P. Strasser, J. Power Sources 196 (2011) 5240–5249.
[14] D.E. Williams, R.C. Newman, Q. Song, R.G. Kelly, Nature 350 (1991) 216.
[15] J. Erlebacher, M.J. Aziz, A. Karma, N. Dimitrov, K. Sieradzki, Nature 410 (2001) 450–453.
[16] Y. Ding, M. Chen, J. Erlebacher, J. Am. Chem. Soc. 126 (2004) 6876–6877.
[17] J. Erlebacher, J. Electrochem. Soc. 151 (2004) C614–C626.
[18] J. Rugolo, J. Erlebacher, K. Sieradzki, Nature 5 (2006) 946–949.
[19] P. Strasser, Rev. Chem. Eng. 25 (2009) 255–295.
[20] P. Strasser, Chem. Ing. Tech. 81 (2009) 573–580.
[21] P. Strasser in, W. Vielstich, H.A. Gasteiger, H. Yokokawa, Handbook of Fuel Cells: Advances in Electrocatalysis, Materials, Diagnostics and Durability, John Wiley & Sons Ltd., Chichester, 2009, pp. 30–47.
[22] R. Srivastava, P. Mani, P. Strasser, J. Power Sources 190 (2009) 40–47.
[23] K.C. Neyerlin, R. Srivastava, P. Strasser, ECS Trans. 16 (2008) 509–514.
[24] P. Strasser, S. Koh, J. Greeley, Phys. Chem. Chem. Phys. 10 (2008) 3670–3683.
[25] R. Makharia, S.S. Kocha, P.T. Yu, M.A. Sweikart, W. Gu, F.T. Wagner, H.A. Gasteiger, ECS Trans. 1 (8) (2006) 3–18.
[26] C.A. Reiser, L. Bregoli, T.W. Patterson, J.S. Yi, J.D. Yang, M.L. Perry, T.D. Jarvi, Electrochem. Solid State Lett. 8 (2005) A273–A276.
[27] E. Antolini, J.R.C. Salgado, E.R. Gonzalez, J. Power Sources 160 (2006) 957–968.
[28] A. Marcu, G. Toth, S. Kundu, L.C. Colmenares, R.J. Behm, J. Power Sources, submitted for publication.
[29] P. Mani, R. Srivastava, P. Strasser, ECS Trans. 11 (2007) 933–940.
[30] P. Mani, R. Srivastava, P. Strasser, J. Phys. Chem. 112 (2008) 2770–2778.
[31] P. Strasser, S. Koh, C. Yu, ECS Trans. 11 (2007) 167–180.
[32] Z. Liu, C. Yu, I.A. Rusakova, D. Huang, P. Strasser, Top. Catal. 49 (2008) 241–250.
[33] Z. Liu, S. Koh, C. Yu, P. Strasser, J. Electrochem. Soc. 154 (2007) B1192–B1199.
[34] S. Koh, C. Yu, P. Strasser, ECS Trans. 11 (2007) 205–215.
[35] H.A. Gasteiger, N.M. Markovi, Science 324 (2009) 48–49.
[36] M. Oezaslan, F. Hasche, P. Strasser, ECS Trans. 33 (2010) 333–341.
[37] P. Mani, R. Srivastava, P. Strasser, J. Power Sources 196 (2011) 666–673.
[38] P. Strasser, J.D. Stemwedel, J. Ross, J. Phys. Chem. 97 (1993) 2851–2862.
[39] S. Koh, N. Hahn, C. Yu, P. Strasser, J. Electrochem. Soc. 155 (2008) B1281–B1288.
[40] P. Strasser, M. Ata, J. Phys. Chem. 102 (1998) 4131–4134.
[41] K. Yaccato, R. Carthart, A. Hagemeyer, A. Lesik, P. Strasser, A. Volpe, H. Turner, H. Weinberg, R. Grassselli, C. Brooks, Appl. Catal. 296 (2005) 30–48.
[42] T.J. Schmidt, H.A. Gasteiger, G.D. Sta, P.M. Urban, D.M. Kolb, R.J. Behm, J. Electrochem. Soc. 145 (1998) 2354–2358.
[43] Z. Jusys, J. Kaiser, R.J. Behm, Phys. Chem. Phys. 3 (2001) 4650–4660.
[44] T. Biegler, D.A.J. Rand, R. Woods, J. Electroanal. Chem. 29 (1971) 269–277.
[45] P. Strasser, P. Manni, R. Sirivastava, US Patent Application 20090098420 (2008).
[46] F. Hasche, M. Oezaslan, P. Strasser, Chem. Cat. Chem. 3 (2011) 1–10.
[47] N. Linse, L. Gubler, G.G. Scherer, A. Wokaun, Electrochim. Acta 56 (2011) 7541–7549.
[48] R.L. Borup, J.R. Davey, F.H. Garzon, D.L. Wood, M.A. Inbody, J. Power Sources 163 (2006) 76–81.
[49] A. Horky, K. Beverage, O. Polevaya, Y. Shi, Proceedings of the Fuel Cells Durability, Washington, DC, first ed., 2006, pp. 133–150.
[50] P.J. Ferreira, G.J. la O', Y. Shao-Horn, D. Morgan, R. Makharia, S. Kocha, H.A. Gasteiger, J. Electrochem. Soc. 152 (11) (2005) A2256–A2271.
[51] Y. Shao-Horn, W.C. Sheng, S. Chen, P.J. Ferreira, E.F. Holby, D. Morgan, Top. Catal. 46 (2007) 285–305.
[52] W. Bi, T.F. Fuller, J. Electrochem. Soc. 155 (2) (2008) B215–B221.
[53] W. Ostwald, Lehrbuch der Allgemeinen Chemie, Engelmann, Leipzig, 1896, pp. 444–465.